ELSEVIER

Physica D 125 (1999) 241–259

PHYSICA D

Synchronizing multiple chaotic maps with a randomized scalar coupling

Ali A. Minai *, Tirunelveli Anand

Department of Electrical & Computer Engineering and Computer Science, University of Cincinnati, Cincinnati, OH 45221-0030, USA

Received 25 February 1998; received in revised form 25 August 1998; accepted 28 August 1998
Communucated by A.M. Albano

Abstract

Synchronization between chaotic systems has recently been a topic of great interest among physicists and engineers. In addition to theoretical results, a number of applications in communications and control have also been proposed. We have previously shown that identical chaotic maps can, under certain conditions, be synchronized by a common noise-like input. This raises the question whether the chaotic output from a map can synchronize other maps to itself. In this paper, we present results on the synchronization of two identical maps where the output of one map is used to drive both maps. We then apply this method to synchronizing identical but internally inhomogeneous populations of chaotic oscillators using a randomly constructed scalar coupling signal, which tends to white noise as the number of oscillators increases. Such a system may have applications in secure communication.

PACS: 05.45.+b; 43.72.+q; 07.05.Pj

Keywords: Synchronization; Chaotic oscillators; Coupled oscillators; Coupled maps

1. Introduction

Synchronization among chaotic systems has received considerable attention in recent years, with a large body of results on theory [1,2] and applications [3–16]. The first major results were obtained by Pecora and Carroll [1,2], who demonstrated that two identical chaotic systems (such as the Lorenz system) could be synchronized if one of the phase variables in the second system – called the *response system* – was replaced by the corresponding phase variable from the first system – called the *drive system*. The primary requirement was that the subsystem comprised by the unreplaced phase variables of the response system be stable in its own right. Subsequently, several researchers presented schemes for synchronizing chaotic and hyperchaotic systems by control techniques [12,13,16–18].

Synchronization between two bidirectionally coupled discrete-time maps was first studied by Yamada and Fujisaka [19] using the form

$$x_{n+1} = \phi(x_n) + \zeta[\phi(y_n) - \phi(x_n)], \tag{1}$$

$$y_{n+1} = \phi(y_n) + \zeta[\phi(x_n) - \phi(y_n)], \tag{2}$$

* Corresponding author. Tel.: +1-513-556-4783; fax: +1-513-556-7326; e-mail: ali.minai@uc.edu

0167-2789/99/$ – see front matter
PII: S0167-2789(98)00247-4

where $\phi(\ )$ is the nonlinear map. They showed that x_n and y_n synchronize if ζ is large enough. These results were further extended in [20,21]. Bidirectionally coupled maps have also been investigated by Wang [22]. Large systems of coupled maps – called *coupled map lattices (CMLs)* and *globally coupled maps (GCMs)* – have been studied in detail by Kaneko and others [23–26], and a great variety of turbulent, clustering, and synchronized regimes have been found for these. Synchronization has also been investigated in diffusively and globally connected arrays of chaotic systems [27–30].

The issue of synchronization in unidirectionally coupled maps has recently been addressed by several researchers [16,31–38]. In most of these cases, the coupling is implicitly or explicitly diffusive, i.e., it depends on the difference between the states of the driving and response systems [39]. Pecora et al. [36,38] use a general method called synchronous substitution [40] to synchronize unidirectionally coupled volume-preserving and volume-expanding piecewise linear maps. This method is also based on (possibly nonlinear) feedback control. Güémez and Matías [33] use direct partial substitution of a response variable by the corresponding drive variable, which sometimes leads to synchronization. Zonghua and Shigang [41] use periodic driving to synchronize two conservative maps.

In recent reports [42,43], we have shown that identical chaotic maps can, in some cases, be synchronized by a common noise-like input via a coalescence mechanism [44–46]. In this paper, we refine our analysis and show that the same effect can be used to synchronize unidirectionally coupled systems, with the aperiodic output of the driving system used as the common input. The system we study can also be given a diffusive formulation, but the synchronization mechanism does not depend on the differential term, which makes this method very flexible. In particular, when the driving and response systems consist of many subsystems, the coupling signal may be a *random function* of the driving system variables, making it truly noise-like. This could be an advantage in secure communication applications [38].

2. Single system synchronization

The systems we consider use a scalar signal from the drive system as input to *both* the response and the drive systems. Thus, both systems can be seen as autonomous maps with identical inputs. The map we use is based on a discrete-time neural oscillator studied by Wang [22,47]:

$$z_{t+1} = f(z_t) = \tanh[\mu A z_t] - \tanh[\mu B z_t], \tag{3}$$

where $A, B > 0$, $A/B \geq 2$. If μ is large enough, the map is chaotic [47]. When an external input, u, is added to the system, we get

$$z_{t+1} = f(z_t) = \tanh[\mu(A z_t + u)] - \tanh[\mu B z_t]. \tag{4}$$

It can be shown that, if the map is chaotic for $u = 0$, it undergoes a period-halving cascade with increasing u, eventually leading to a period-2 regime [48]. If u is time varying, the system is intermittently chaotic and periodic. Two identical systems driven by such an input become synchronized through rapid coalescence [42].

To study synchronization between coupled maps, we first consider the one-dimensional system

$$z^{\mathrm{d}}_{t+1} = \tanh[\mu(A z^{\mathrm{d}}_t + \beta z^{\mathrm{d}}_t)] - \tanh[\mu B z^{\mathrm{d}}_t], \tag{5}$$

$$z^{\mathrm{r}}_{t+1} = \tanh[\mu(A z^{\mathrm{r}}_t + \beta z^{\mathrm{d}}_t)] - \tanh[\mu B z^{\mathrm{r}}_t], \tag{6}$$

where superscripts d and r indicate the drive and response systems, respectively, and β is the coupling strength. Defining $e_t = z^{\mathrm{d}}_t - z^{\mathrm{r}}_t$, it is clear that $e_t = 0$ is an invariant manifold of the system. However, synchronization does not occur because the conditions necessary for coalescence [42] of orbits are not satisfied. These are:

(i) The conditional Lyapunov exponents of both systems must be negative.
(ii) The dynamics of the systems must include intermittent chaotic and periodic regimes.

In the system above, the drive map can be written as

$$z^{\mathrm{d}}_{t+1} = \tanh[\mu(A+\beta)z^{\mathrm{d}}_t] - \tanh[\mu B z^{\mathrm{d}}_t], \tag{7}$$

which is just an autonomous map with either wholly chaotic or wholly periodic dynamics. Thus, coalescence to identical trajectories will not occur except by accident.

Systems with differential feedback, as in [34]

$$z^{\mathrm{d}}_{t+1} = f(z^{\mathrm{d}}_t), \qquad z^{\mathrm{r}}_{t+1} = f(z^{\mathrm{r}} + \epsilon[z^{\mathrm{d}}_t - z^{\mathrm{r}}_t]) \tag{8}$$

or [35]

$$z^{\mathrm{d}}_{t+1} = f(z^{\mathrm{d}}_t), \qquad z^{\mathrm{r}}_{t+1} = f(z^{\mathrm{r}}_t) + \epsilon[f(z^{\mathrm{d}}_t) - f(z^{\mathrm{r}}_t)] \tag{9}$$

do synchronize if ϵ is large enough. However, the extension of these methods to multiple maps is problematic, requiring precisely tuned [16,17] and possibly high-dimensional [12,17,32] coupling. Also, note that both the above systems have the trivial "optimal" coupling $\epsilon = 1.0$.

We look next at the case where the drive and response systems are two-dimensional:

$$\begin{aligned}
y^{\mathrm{d}}_{t+1} &= f_y(y^{\mathrm{d}}_t, z^{\mathrm{d}}_t) = \tanh[\mu_y(Cy^{\mathrm{d}}_t + \beta z^{\mathrm{d}}_t)] - \tanh[\mu_y D y^{\mathrm{d}}_t],\\
z^{\mathrm{d}}_{t+1} &= f_z(z^{\mathrm{d}}_t, y^{\mathrm{d}}_{t+1}) = \tanh[\mu_z(Az^{\mathrm{d}}_t + \alpha y^{\mathrm{d}}_{t+1})] - \tanh[\mu_z B z^{\mathrm{d}}_t],\\
y^{\mathrm{r}}_{t+1} &= f_y(y^{\mathrm{r}}_t, z^{\mathrm{d}}_t) = \tanh[\mu_y(Cy^{\mathrm{r}}_t + \beta z^{\mathrm{d}}_t)] - \tanh[\mu_y D y^{\mathrm{r}}_t],\\
z^{\mathrm{r}}_{t+1} &= f_z(z^{\mathrm{r}}_t, y^{\mathrm{r}}_{t+1}) = \tanh[\mu_z(Az^{\mathrm{r}}_t + \alpha y^{\mathrm{r}}_{t+1})] - \tanh[\mu_z B z^{\mathrm{r}}_t],
\end{aligned} \tag{10}$$

where α and β are fixed parameters. The drive and response systems – which we will term oscillators – can each be seen as two chain-connected maps. The coupling between the systems is only through βz^{d}_t. Note also that, while the corresponding maps in each oscillator are identical, the two maps within each oscillator may be different, provided they are both chaotic. We assume all maps to be identical for clarity. Once again, $y^{\mathrm{r}}_t = y^{\mathrm{d}}_t$, $z^{\mathrm{r}}_t = z^{\mathrm{d}}_t$ is an invariant manifold. Henceforth, this will be termed the *synchronization manifold (SM)*. We investigate its stability numerically to conclude that it is stable in a broad α–β domain, implying that synchronization is stable and generic in this regime.

We begin analysis by rewriting the equation for the y maps as

$$\begin{aligned}
y^{\mathrm{d}}_{t+1} &= \tanh[\mu_y(Cy^{\mathrm{d}}_t + \beta z^{\mathrm{d}}_t)] - \tanh[D\mu_y y^{\mathrm{d}}_t],\\
y^{\mathrm{r}}_{t+1} &= \tanh[\mu_y(Cy^{\mathrm{r}}_t + \beta z^{\mathrm{r}}_t + \beta(z^{\mathrm{d}}_t - z^{\mathrm{r}}_t))] - \tanh[D\mu_y y^{\mathrm{r}}_t],
\end{aligned} \tag{11}$$

showing that the y maps become decoupled when the z maps synchronize. Substituting this into the map for z^{r}_{t+1}, we see that the same is true of the z maps. In this, our system is like all other diffusively coupled systems. The key difference, however, is that y_{d} and y_{r} can synchronize *even when* z^{d} *and* z^{r} *are not synchronized*, since both are driven by the same signal, z^{d}_t. The mechanism for this synchronization is not differential feedback but, as we have discussed elsewhere [42,43], the repeated coalescence and phase-mixing produced by jumps between periodic and chaotic dynamics in response to the input each oscillator receives. Thus, y^{d} and y^{r} synchronize first in response to the common input βz^{d}_t, and then synchronize z^{d} and z^{r}, also through the repeated coalescence mechanism. Once the z's are synchronized, the drive and response systems become decoupled and follow synchronized aperiodic trajectories.

To investigate the stability of the synchronization, we define the error phase variables:

$$e^y_t = y^{\mathrm{d}}_t - y^{\mathrm{r}}_t, \qquad e^z_t = z^{\mathrm{d}}_t - z^{\mathrm{r}}_t, \tag{12}$$

whose dynamics along a particular $(y^{\mathrm{d}}_t, z^{\mathrm{d}}_t)$ trajectory is given by

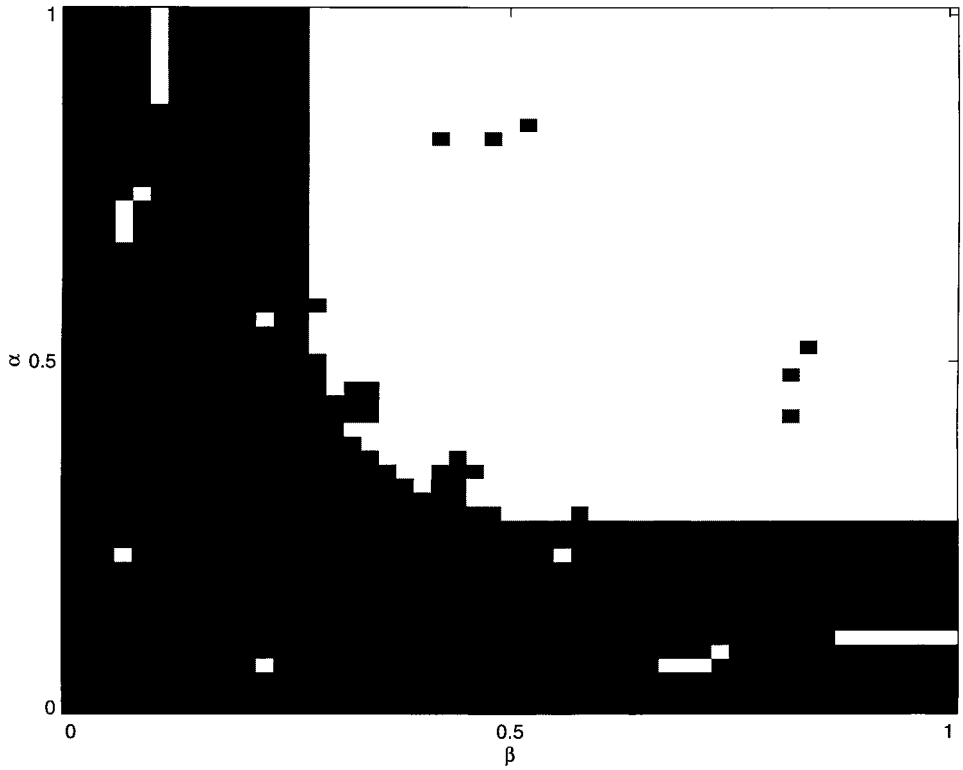

Fig. 1. The signs of the empirically determined conditional Lyapunov exponents (CLEs) for the two-dimensional system plotted in the α–β space. White indicates that CLEs for both e^y and e^z are negative. The parameters are $\mu_y = \mu_z = 5.0$, $A = C = 5.0$, $B = D = 1.0$. Each data point was averaged over 10 independent runs, each 50 000 steps long, with the last 40 000 steps used for calculating the CLEs.

$$e^y_{t+1} = F_y(e^y_t, e^z_t) = \tanh[\mu_y(Cy^{\mathrm{d}}_t + \beta z^{\mathrm{d}}_t)] - \tanh[\mu_y D y^{\mathrm{d}}_t] - \tanh[\mu_y(C(y^{\mathrm{d}}_t - e^y_t) + \beta z^{\mathrm{d}}_t)] + \tanh[\mu_y D(y^{\mathrm{d}}_t - e^y_t)], \tag{13}$$

$$e^z_{t+1} = F_z(e^y_t, e^z_t) = \tanh[\mu_z(Az^{\mathrm{d}}_t + \alpha f_y(y^{\mathrm{d}}_t, z^{\mathrm{d}}_t)] - \tanh[\mu_z B z^{\mathrm{d}}_t] - \tanh[\mu_z(A(z^{\mathrm{d}}_t - e^z_t) + \alpha f_y(y^{\mathrm{d}}_t - e^y_t, z^{\mathrm{d}}_t))] + \tanh[\mu_z B(z^{\mathrm{d}}_t - e^z_t)]. \tag{14}$$

The Jacobian along this trajectory is given by

$$\begin{bmatrix} \partial F_y/\partial e^y & \partial F_y/\partial e^z \\ \partial F_z/\partial e^y & \partial F_z/\partial e^z \end{bmatrix}. \tag{15}$$

Since $\partial F_y/\partial e^z = 0$, the eigenvalues of the array are simply the diagonal elements, which allows the numerical calculation of the two transverse conditional Lyapunov exponents (CLEs) for the (e^y, e^z) system:

$$\Lambda_y = \lim_{T\to\infty} T^{-1} \sum_{t=\tau}^{\tau+T-1} \ln\left|\partial F_y/\partial e^y\right|,$$

$$\Lambda_z = \lim_{T\to\infty} T^{-1} \sum_{t=\tau}^{\tau+T-1} \ln\left|\partial F_z/\partial e^z\right|, \tag{16}$$

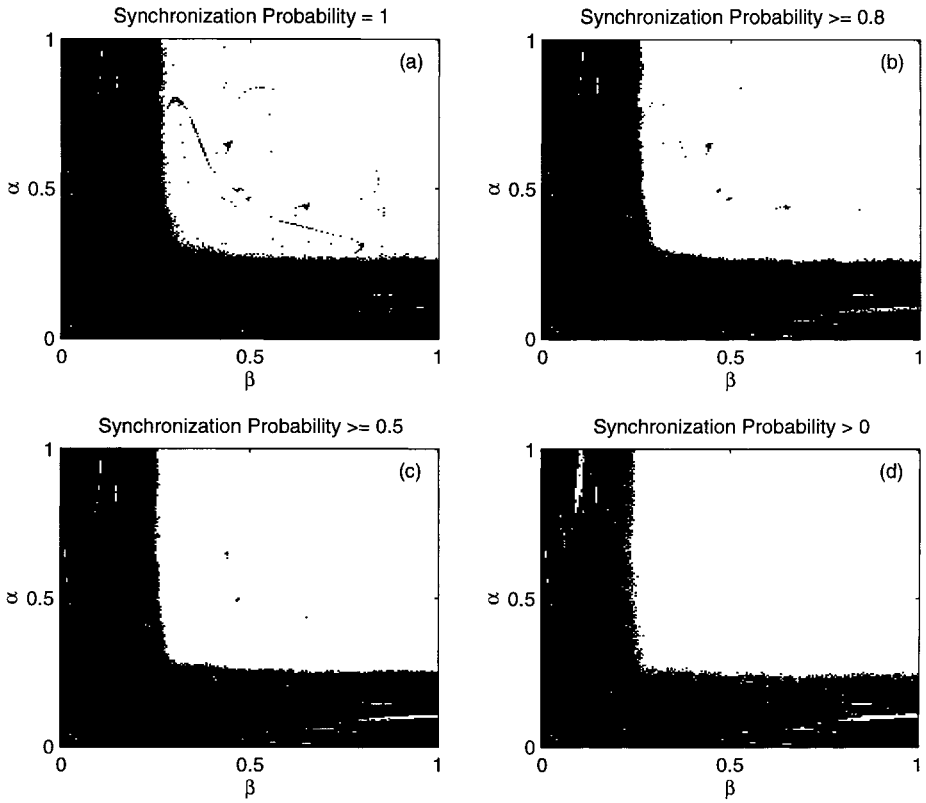

Fig. 2. The actual, empirically determined domains of synchronization for two y–z oscillators with parameters set as in Fig. 1. Each data point is based on 20 independent runs of 5000 steps each. White indicates that synchronization occurred within 5000 steps with probability 1.0 (a); > 0.8 (b); ≥ 0.5 (c) and > 0 (d).

where the derivatives are evaluated at $(e^y, e^z) = (0, 0)$. Fig. 1 shows the sign of the maximal CLE over a part of the α–β space for a set of oscillators. Clearly, there is a large region where both Lyapunov exponents are negative, and synchronization would be stable.

3. Coalescence and global stability

Stability analysis based on transverse CLEs has two important caveats. First, it only indicates the local stability of synchronization but not whether synchronization would emerge when the system starts from arbitrary initial conditions. Second, since the CLEs are averaged quantities, negative CLEs only imply movement towards synchronization over time. It is quite possible for a trajectory perturbed off the SM to move away from it for a time. In other words, negative CLEs do not preclude finite-time episodes of trajectory separation – only long-term coalescence. Such finite-time desynchronizations are an example of "bubbling" [35,39], and reflect the fact that the neighborhood of the SM contains a set which repels orbits away from the SM [20,49,50].

Finding analytical conditions for global stability is, in general, quite difficult, and most work on synchronization has focused on numerical evaluation of local stability (except in a few tractable cases [20,35,49]). Following this practice, we test for synchronization through simulations for the parameter values used in the CLE analysis (above). The results, averaged over 20 initial conditions for each setting of α and β, are shown in Fig. 2. It shows that synchronization actually does emerge almost everywhere in the region with negative CLEs. Also, as shown in

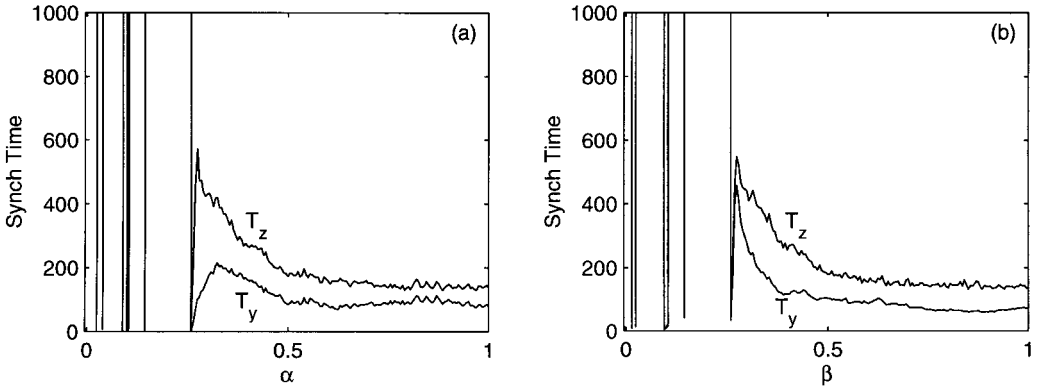

Fig. 3. Averaged synchronization times for the y and z maps in the system from Fig. 2. In graph (a), the average is over all values of β that produced synchronization with probability 1.0 (over 20 runs). In graph (b), the average is over all such α values. Note that the y maps always synchronize first, showing that $z_t^{\mathrm{d}} - z_t^{\mathrm{r}}$ need not be 0 for y-map synchronization.

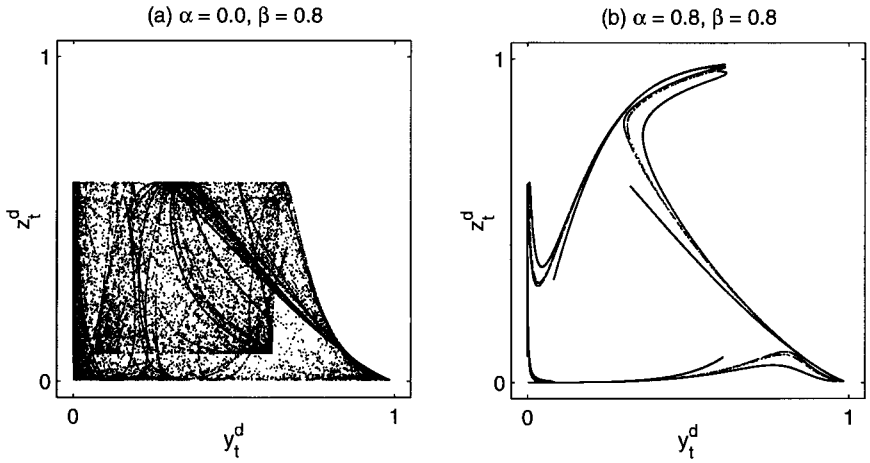

Fig. 4. Phase-space behavior of the autonomous drive oscillator with $\mu_y = \mu_z = 5.0$, $A = C = 5.0$, and $B = D = 1.0$. The $z \to y$ coupling, β, is 0.8 in both cases. The $y \to z$ coupling is 0 for (a) and 0.8 for (b). Thus, the z-map for the system shown in (a) is autonomous, and z_t^{d} and z_t^{r} would not synchronize in this case. Both cases lead to synchronization of y_t^{d} and y_t^{r}. 10^5 points are plotted in each graph.

Fig. 3, the mean synchronization times are quite short (a few hundred steps), and synchronization is driven by coalescence in the y maps. Of course, the fact that synchronization occurs does not imply that phenomena such as bubbling are excluded. Indeed, the addition of an independent noise in the system does produce intermittent bursts of desynchronization, but the fact that these bursts have finite duration suggests that the SM is the only attractor in the negative CLE regime.

To further explore these issues, we focus on the synchronization of y_t^{d} and y_t^{r}, and consider the subsystem given by

$$y_{t+1}^{\mathrm{d}} = f_y(y_t^{\mathrm{d}}, z_t^{\mathrm{d}}) = \tanh[\mu_y(Cy_t^{\mathrm{d}} + \beta z_t^{\mathrm{d}})] - \tanh[\mu_y D y_t^{\mathrm{d}}],$$

$$z_{t+1}^{\mathrm{d}} = f_z(z_t^{\mathrm{d}}, y_{t+1}^{\mathrm{d}}) = \tanh[\mu_z(Az_t^{\mathrm{d}} + \alpha y_{t+1}^{\mathrm{d}})] - \tanh[\mu_z B z_t^{\mathrm{d}}],$$

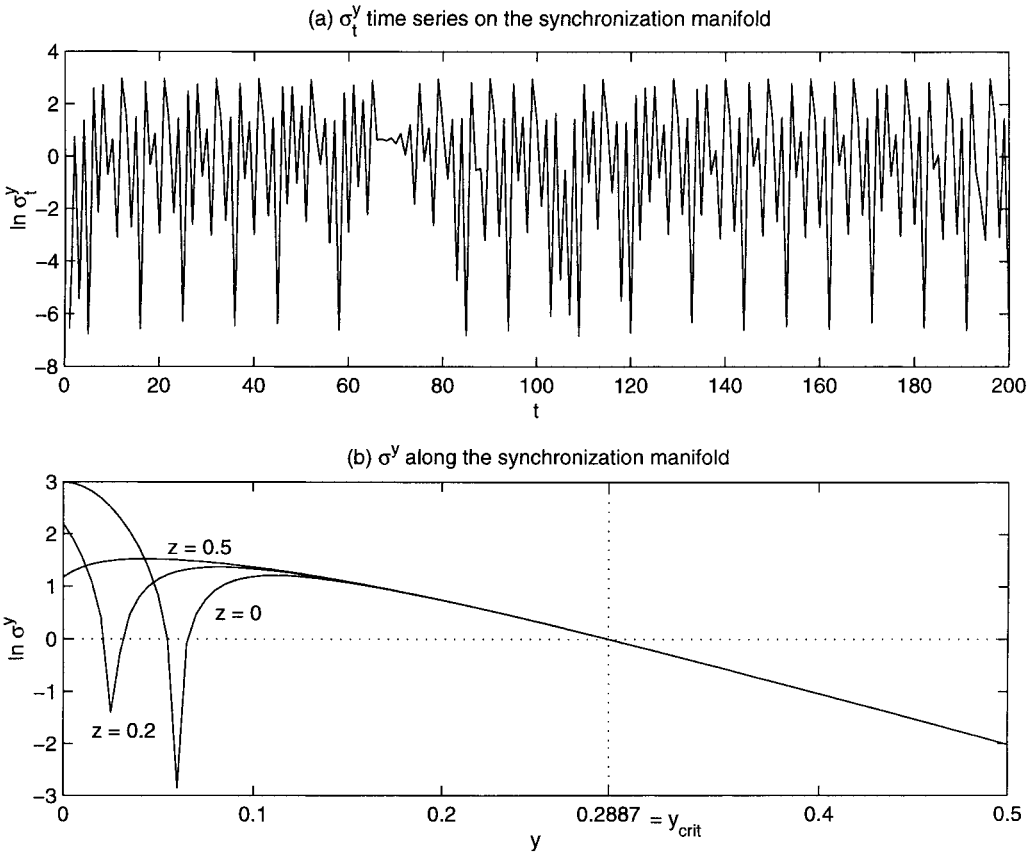

Fig. 5. Graph (a) shows the time series of $\ln \sigma_t^y$ for the system from Fig. 4(b). The CLE, Λ_y, is obtained as the mean of the plotted quantity as $t \to \infty$, and is negative for this system ($\Lambda_y = -0.45$). However, short-time averages of $\ln(\sigma_t^y)$ can exceed 0. Graph (b) plots $\ln(\sigma^y)$ against y along the synchronization manifold ($y^{\mathrm{d}} = y^{\mathrm{r}} = y$) for three values of z. Parameters are as for Graph (a).

$$\begin{aligned} e_{t+1}^y &= F_y(e_t^y, y_t^{\mathrm{d}}, z_t^{\mathrm{d}}) \\ &= \tanh[\mu_y(Cy_t^{\mathrm{d}} + \beta z_t^{\mathrm{d}})] - \tanh[\mu_y D y_t^{\mathrm{d}}] \\ &\quad - \tanh[\mu_y(C(y_t^{\mathrm{d}} - e_t^y) + \beta z_t^{\mathrm{d}})] + \tanh[\mu_y D(y_t^{\mathrm{d}} - e_t^y)]. \end{aligned} \tag{17}$$

Note that z_t^{r} plays no role in the synchronization of the y variables, and can be ignored here. Once y_t^{d} and y_t^{r} synchronize, the same system as above can be used to analyze synchronization between z_t^{d} and z_t^{r}, now driven by the common y-signal. For concreteness, we take $\mu_y = \mu_z = 5.0$, $A = C = 5.0$, $B = D = 1.0$, though the results are qualitatively the same if the parameters are set such that the maps are chaotic when $\alpha = \beta = 0$. Since y_t^{d} and z_t^{d} are independent of y_t^{r}, the dynamics in the $(y^{\mathrm{d}}, z^{\mathrm{d}})$-plane is independent of e_t^y. Fig. 4 shows the invariant sets to which the $(y^{\mathrm{d}}, z^{\mathrm{d}})$ dynamics converges for $\alpha = 0.0$, $\beta = 0.8$, and $\alpha = \beta = 0.8$. The only fixed point of the error map, $F_y(e^y, y^{\mathrm{d}}, z^{\mathrm{d}})$, or its iterates that is sufficiently invariant to y^{d} and z^{d} is $e^y = 0$. Also, the boundedness of the $\tanh(\ )$ function means that the dynamics is confined to a bounded region, B, of the $(e^y, y^{\mathrm{d}}, z^{\mathrm{d}})$ space. Thus, when the dynamics in $(y^{\mathrm{d}}, z^{\mathrm{d}})$-space is aperiodic, e_t^y converges to 0 (synchronization) or to an aperiodic trajectory, depending on the CLE Λ_y. Defining

$$\sigma_t^y(e_t^y, y_t^{\mathrm{d}}, z_t^{\mathrm{d}}) = \mid \partial F_y(e_t^y, y_t^{\mathrm{d}}, z_t^{\mathrm{d}})/\partial e^y \mid, \tag{18}$$

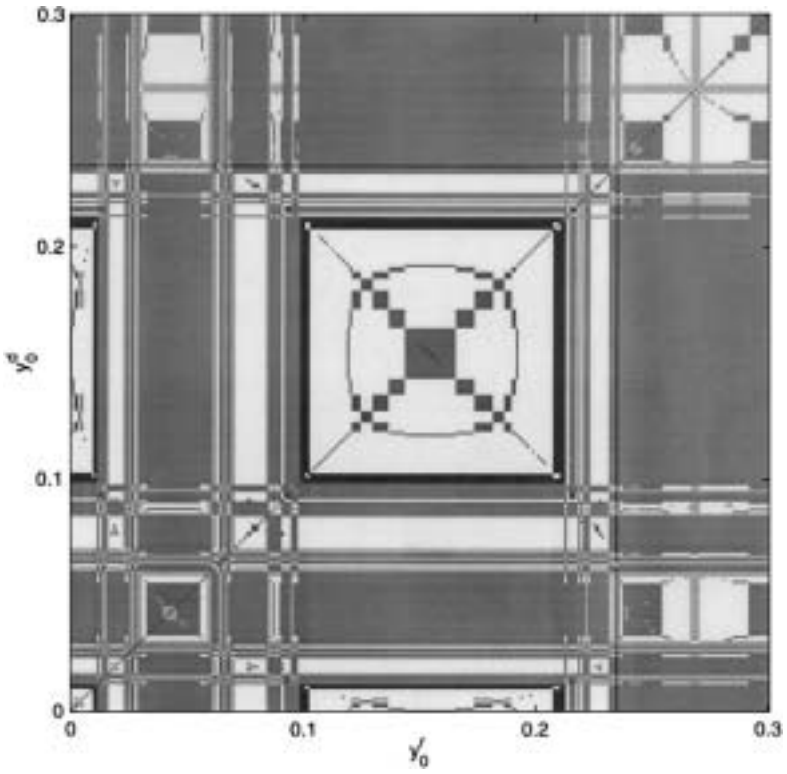

Fig. 6. Synchronization times for trajectories starting at different points in the $(y^{\mathrm{d}}, y^{\mathrm{r}})$-plane. Parameter values are as for Fig. 4(a). All trajectories synchronized to a precision of 10^{-16} within 330 steps. Different gray levels indicate domains with different synchronization times, but there is no correspondence between intensity and time. A fractal strucutre is apparent (see Fig. 8). Resolution along each axis was 0.001.

the CLE is given by

$$\Lambda_y = \langle \ln(\sigma_t^y(0, y_t^{\mathrm{d}}, z_t^{\mathrm{d}}))\rangle = \lim_{T\to\infty} \frac{1}{T}\sum_{t=0}^{T-1} \ln(\sigma_t^y(0, y_t^{\mathrm{d}}, z_t^{\mathrm{d}})). \tag{19}$$

However, as pointed out by Ott and Sommerer [51], a globally negative CLE does not preclude finite-time divergence. To demonstrate this, we plot in Fig. 5(a) the time series of $\ln(\sigma_t^y)$ for part of the trajectory shown in Fig. 4(b) (steps 400–600, when synchronization has already occurred). As the time series shows, coalescence dominates divergence on average, which is why synchronization emerges this case. However, it is also clear that $\langle \ln(\sigma^y)\rangle < 0$ does not preclude finite intervals of times when σ_t^y is above 1. The reason is illustrated by Fig. 5(b), which plots σ^y against y along the SM for different z values. As y_t^{d} and z_t^{d} change, they sample both the positive and negative parts of the $\ln(\sigma^y)$ surface in $(y^{\mathrm{d}}, z^{\mathrm{d}})$-space. Thus, the SM is stable only *on average*, and small amounts of noise can cause occasional brief excursions away from it. This is an instance of "bubbling" as described above. Also, trajectories that approach the SM typically undergo transient divergent episodes on their way to convergence [44,45]. This is discussed in more detail below. Incidentally, as Fig. 5(b) shows, the y^{d} value at which σ^y finally crosses 0 is almost invariant to z^{d} if $\mu_y C$ is large enough, and can be calculated explicitly as

$$y_{\mathrm{crit}} \approx q \ln\left[\frac{1+\sqrt{1-q}}{\sqrt{q}}\right], \tag{20}$$

where

$$q = 1/\mu_y D.$$

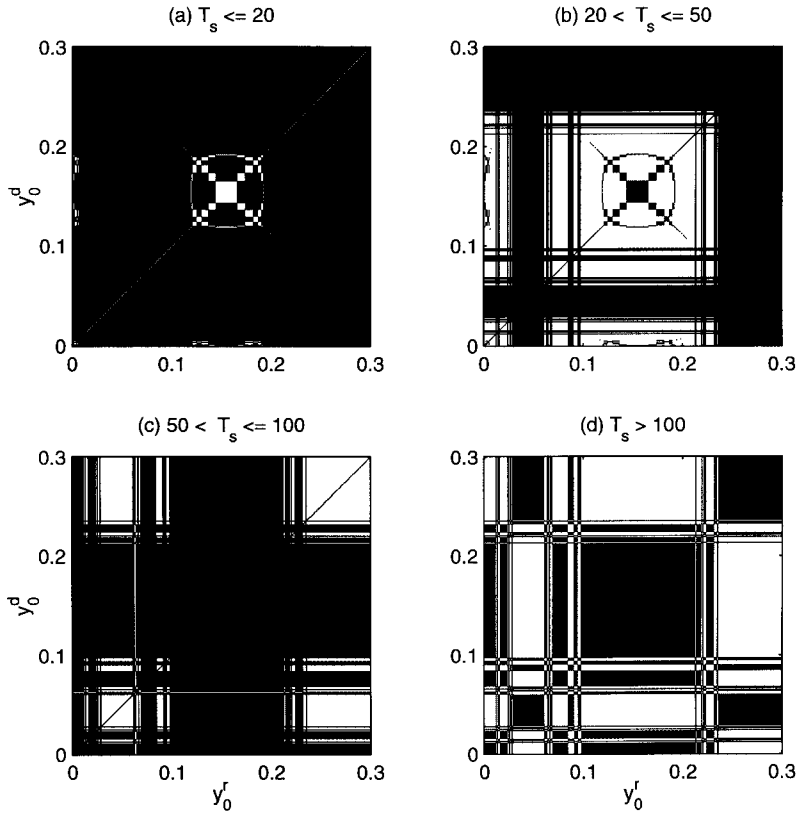

Fig. 7. The same data as in Fig. 6, but thresholded to show regions with synchronization times in four different intervals. White areas represent initial conditions that synchronized within the corresponding time window.

To see this, recall that, for $e^y = 0$, $\partial F_y/\partial e^y = \partial f_y/\partial y$. For large enough $\mu_y C$, $f_y(y) \approx 1 - \tanh(\mu_y D y)$ if y is not too close to 0. The approximation for y_{crit} follows.

A qualitative understanding of the emergence and persistence of synchronization can be obtained by following the behavior of all trajectories in some part of $(y^{\text{d}}, y^{\text{r}})$-space. We look at the evolution of initial conditions in the region $(0 \leq y_0^{\text{d}} \leq 0.3, 0 \leq y_0^{\text{r}} \leq 0.3)$ for $z_0^{\text{d}} = 0.1$ and $\mu_y = \mu_z = 5.0$, $A = C = 5.0$, $B = D = 1.0$, and follow the time required to reach synchronization. Figs. 6 and 7 show the results for the $\alpha = 0.0$, $\beta = 0.8$ case. All initial conditions tried in this case (resolution of 0.001 along each axis) converged within 330 steps, and more than half in 100 steps or less. This provides an indication of how long desynchronization episodes might last. Fig. 8 shows a magnification of the $(0 \leq y_0^{\text{d}} \leq 0.1, 0 \leq y_0^{\text{r}} \leq 0)$ region in Fig. 6 at a resolution of 0.00025. The fractal nature of the synchronization domains is clearly apparent from a comparison of the figures. Fig. 9 shows the synchronization time results for $\alpha = \beta = 0.8$. Here, the dynamics of z^{d} is much more correlated with y^{d} (See Fig. 4(b)), and this asymmetry produces a very different distribution of synchronization times. However, once again, all points do synchronize within 250 steps.

One issue that arises in all numerical studies of chaotic synchronization is that of numerical precision [52,53]. Typically, true synchronization between sub-systems occurs only in the limit of infinite time. However, once the trajectories of the two sub-systems come closer than the precision of the computer representation, they effectively become synchronized for all future times. As discussed by Longa et al. [52], synchronization schemes can be classified into two distinct types: (1) those where the time to synchronization depends linearly on precision; and (2) those where the dependence is exponential. In the latter case [54], synchronization is basically a purely passive epiphenomenon of finite precision: One waits until the trajectories happen to come close enough and become

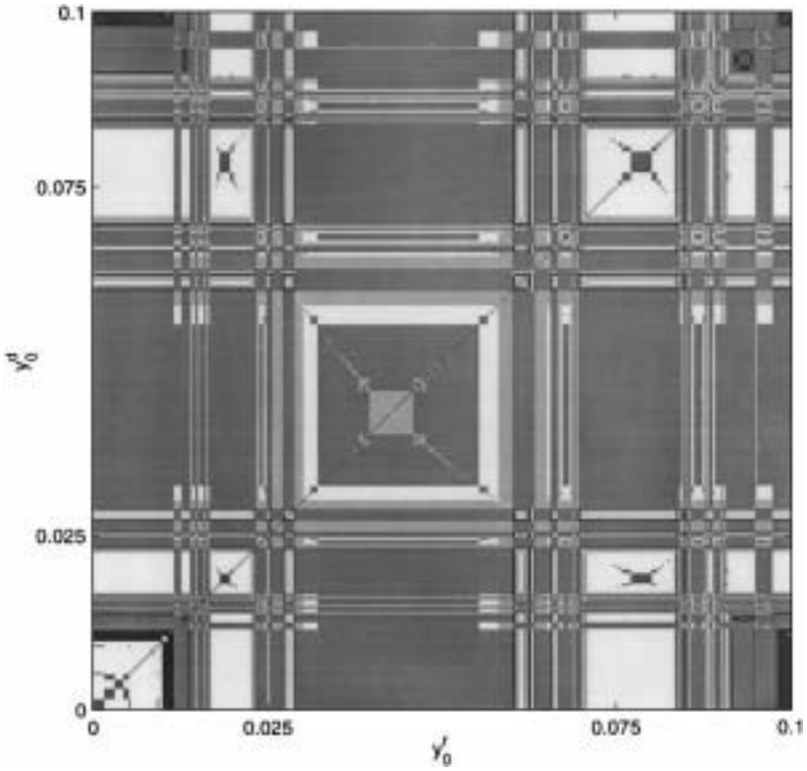

Fig. 8. A magnification of the $[0 \leq y_0^{\mathrm{d}} \leq 0.1, 0 \leq y_0^{\mathrm{r}} \leq 0.1]$ region from Fig. 6. The resolution is 0.00025, and much more structure is visible, indicating the fractal nature of synchronization time domains.

numerically identical. In the former case [1], the trajectories are actually forced together by the dynamics, though in finite time, they only converge to finite precision, and desynchronize occasionally due to bubbling or basin riddling [20,50,51]. For both dissipatively coupled and coalescent systems, the absolute synchronization error, $\mid e_t^y \mid$, is expected to have a power law distribution [20,45,46], indicating that large deviations from the SM are possible but rare.

We investigate these issues for our system by checking the *mean time to first passage*, $t_s(\epsilon)$, defined as the average number of steps it takes for two trajectories – starting from random initial conditions $(y_0^{\mathrm{d}}, z_0^{\mathrm{d}}, y_0^{\mathrm{r}}, z_0^{\mathrm{r}}) \in (0, 1)^4$ – to approach within ϵ of each other. Thus, if synchronization were defined only to resolution ϵ, $t_s(\epsilon)$ would be the approximate synchronization time (we say "approximate" because, in order to get data for various values of ϵ along the same trajectories, we perform all simulations with a fixed precision of 10^{-16}, and the synchronization times obtained with actual limited precision simulations might be shorter than the ones we report). We also look at what happens after the first approach by tracking the subsequent distance between the trajectories. The maximum distance, averaged over random initial conditions, is denoted by $D_{\max}(\epsilon)$, and shows how well coalescence confines trajectories once they have come sufficiently close. Since all simulations are done with a numerical precision of 10^{-16}, $D_{\max}(\epsilon)$ is effectively calculated over the period $t_s(\epsilon)$ to $t_s(10^{-16})$. Once the trajectories come within $\epsilon = 10^{-16}$, they become numerically indistinguishable. The results for the $\alpha = 0.0$, $\beta = 0.8$ and $\alpha = \beta = 0.8$ cases are shown in Figs. 10 and 11, respectively. In both cases, we obtain a dependence of the form $t_s \sim \log(1/\epsilon)$, indicating exponentially convergent trajectories, as would be expected with negative CLEs. These results demonstrate that synchronization to any desired *finite* precision occurs very rapidly and remains stable in the absence of added noise. The linear dependence of t_s on $\log(1/\epsilon)$ indicates true rather than numerical convergence, but finite precision is necessary to prevent bubbling in the long term. This means that coalescence-based synchronization will only be stable on

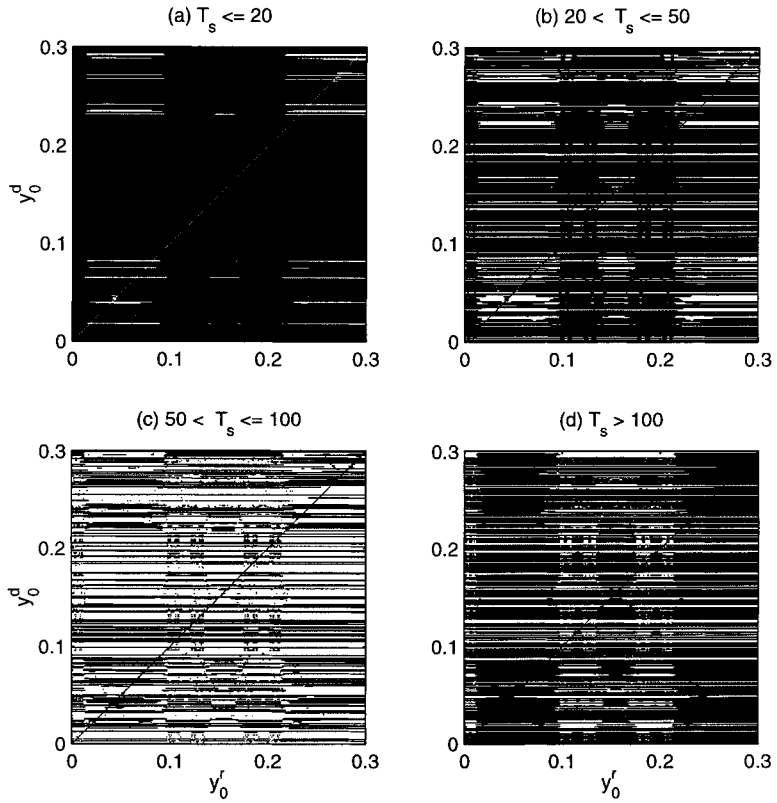

Fig. 9. The analog of Fig. 7 for the $\alpha = \beta = 0.8$ case. Synchronization time domains are now asymmetric because y_t^{d} and z_t^{d} are mutually coupled while y_t^{r} has no coupling with z_t^{d}.

average (i.e., with rare intermittent desynchronizations) for analog physical systems, but will be absolutely stable in applications such as communications and data encryption, which use digital components with limited precision.

To explore the long-term behavior of the system without the limitation imposed by finite precision, we adopt the technique suggested by Yu et al. [44,45], and add a small amount of band-limited independent noise to both y_t^{r} and z_t^{r}. We use uniform noise distributed between $\pm\eta$, $\eta = 10^{-k}$ with $k = 14, 13, 12, 11$, and 10. This prevents perfect numerical synchronization from taking hold, and unmasks the "true" behavior of the system – albeit with added effects due to noise. Fig. 12 shows the distributions of $|\, e_t^y \,|$ and $|\, e_t^z \,|$ obtained for each noise value, and a power law relationship clearly obtains over a significant region. The power law breaks down as the effects of the additive noise become dominant [20,46]. Practically, these results also indicate that additive noise can produce bubbling even with finite precision, with laminar periods whose length depends on the noise power. However, in many cases, this can be mitigated through the use of simple filtering of coupling signals [55]. The discussion of all these phenomena and issues is left to another report.

The analysis and results presented in this section have shown that coalescence-based synchronization is an interesting phenomenon, with potential utility in certain situations. However, synchronization methods based on differential feedback are more stable, and one may ask if coalescence-based methods possess any advantage. The answer lies in the fact that coalescence in response to aperiodic driving is very robust to the actual driving signal. Feedback-based methods require a very precise coupling signal to be sent to the response system, and obtaining this signal can be difficult – especially as the dimensionality of the systems becomes large. The coupling signal that is communicated (to both drive and response systems) for coalescence need only satisfy some very broad statistical constraints [42,43]. Indeed, it need not even come from within the system, and could be external "noise" [55].

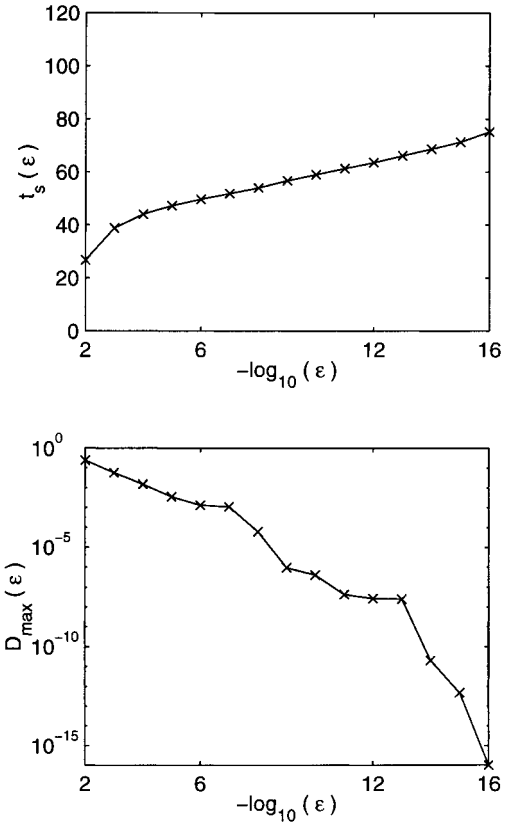

Fig. 10. First passage time and subsequent maximum deviation as a function of synchronization tolerance, ϵ, for y_t^{d} and y_t^{r}. The system parameters are as in Fig. 4(a), with $\alpha = 0.0$ and $\beta = 0.8$. The simulations were all done at a precision of 1^{-16}. Note the linear dependence of t_s on $-\log_{10}(\epsilon)$. Each point was averaged over 500 random initial conditions.

As shown in Section 4, this lack of need for precise tuning allows us to use the same coupling signal – generated randomly within the system – to synchronize large populations of diverse oscillators. The price paid for this freedom from tuning is that the synchronization is less robust than in the feedback case, since the force maintaining it – coalescence on average – is weaker than explicit feedback control.

4. Multiple system synchronization

One of the most interesting applications for the method described above is that it can be used to synchronize corresponding pairs in two mutually identical but internally inhomogeneous populations of oscillators using a random scalar signal from the driving population to the response population. Such synchronization has potential applications in spread-spectrum communications [55,56].

Consider two identical populations of oscillators, $G^{\mathrm{d}} = \{(y_t^{\mathrm{d}_k}, z_t^{\mathrm{d}_k})\}$ and $G^{\mathrm{r}} = \{(y_t^{\mathrm{r}_k}, z_t^{\mathrm{r}_k})\}$, where $k = 1, \ldots, N$ indexes the individual oscillator pairs. The system is shown in Fig. 13. The oscillators within each population may all be different, making it an inhomogeneous population. However, corresponding oscillators across the populations are identical. We assume that parameters are set such that all oscillators are intrinsically chaotic. The synchronizing signal is chosen to be

$$s_t = g(z_t^{\mathrm{d}_1}, \ldots, z_t^{\mathrm{d}_N}) = z_t^{\mathrm{d}_{q_t}}, \tag{21}$$

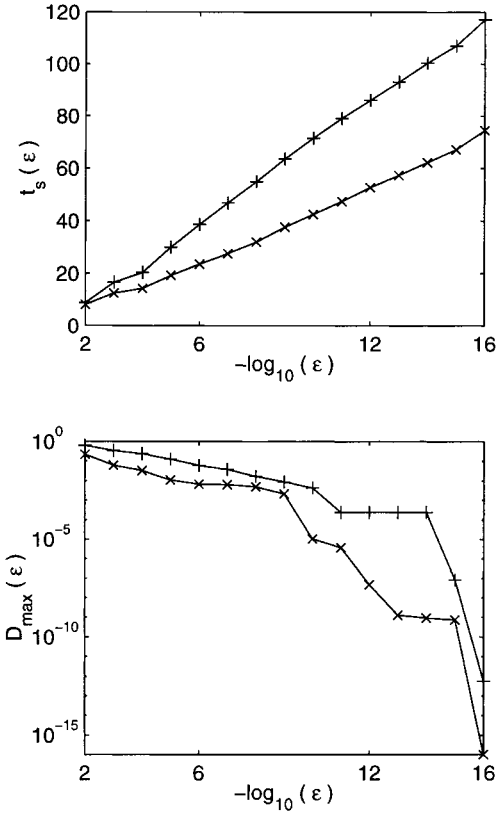

Fig. 11. First passage time and subsequent maximum deviation as a function of synchronization tolerance, ϵ, for $y_t^{\mathrm{d}} - y_t^{\mathrm{r}}(\times)$ and $z_t^{\mathrm{d}} - z_t^{\mathrm{r}}(+)$. The system parameters are as in Fig. 4(b), with $\alpha = \beta = 0.8$. The simulations were all done at a precision of 10^{-16}. While the z-maps take longer to synchronize, the dependence of t_s on resolution is linear for both cases. Each point was averaged over 500 random initial conditions.

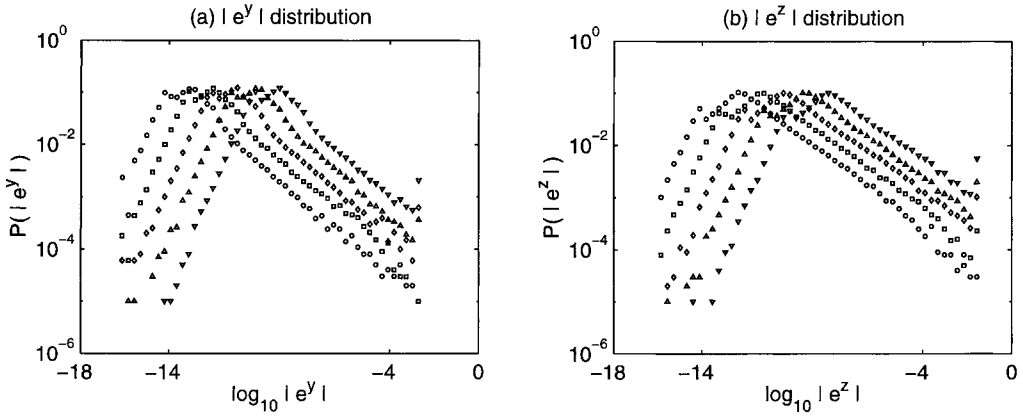

Fig. 12. Distribution of $|e_t^y|$ and $|e_t^z|$ with additive uniform noise $\sim \pm\eta$. In all cases, system parameters are as in Fig. 4(b). The noise widths are: $\log_{10}(\eta) = -14$ (○), -13 (□), -12 (◇), -11 (△), and -10 (▽). Each distribution is calculated using 99 500 points.

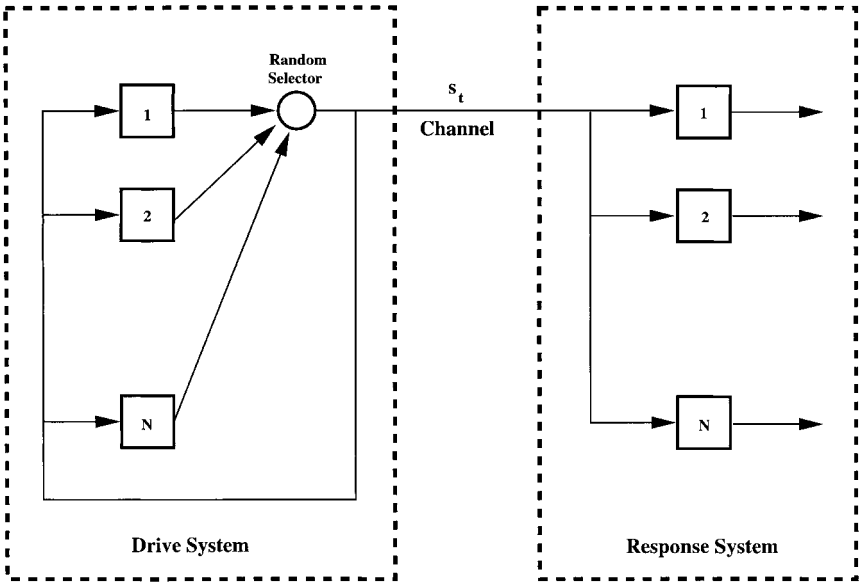

Fig. 13. System for synchronizing multiple oscillators. Each square represents a 2-map y–z oscillator. Identically numbered oscillators in the drive and response systems are identical, but the oscillators within each system may be different, provided that they are all intrinsically chaotic. The output signal for each oscillator is the response of its z-map. The random selector is a switch that, at each step, connects the output of a randomly chosen drive oscillator with the channel, producing the random signal s_t.

where $q_t \in \{1, \ldots, N\}$ is chosen randomly at each step with a uniform distribution. This signal is provided as input to the y component of each oscillator. Note that, unlike the oscillator arrays in [56], G^{d} and G^{r} are not coupled map lattices, but are closer to a globally coupled map network with sparse random time-varying connectivity. Also, in contrast to [56], the arrays are connected only by a scalar channel.

The equations for the kth oscillator pair can be written as:

$$y_{t+1}^{\mathrm{d}_k} = \tanh\left[\mu_{y_k}(C_k y_t^{\mathrm{d}_k} + \beta z_t^{\mathrm{d}_{q_t}})\right] - \tanh\left[\mu_{y_k} D_k y_t^{\mathrm{d}_k}\right],$$

$$z_{t+1}^{\mathrm{d}_k} = \tanh\left[\mu_{z_k}(A_k z_t^{\mathrm{d}_k} + \alpha y_{t+1}^{\mathrm{d}_k})\right] - \tanh\left[\mu_{z_k} B_k z_t^{\mathrm{d}_k}\right],$$

$$y_{t+1}^{\mathrm{r}_k} = \tanh\left[\mu_{y_k}(C_k y_t^{\mathrm{r}_k} + \beta z_t^{\mathrm{r}_{q_t}} + \beta(z_t^{\mathrm{d}_{q_t}} - z_t^{\mathrm{r}_{q_t}}))\right] - \tanh\left[\mu_{y_k} D_k y_t^{\mathrm{r}_k}\right],$$

$$z_{t+1}^{\mathrm{r}_k} = \tanh\left[\mu_{z_k}(A_k z_t^{\mathrm{r}_k} + \alpha(\tanh\left[\mu_{y_k}(C_k y_t^{\mathrm{r}_k} + \beta z_t^{\mathrm{r}_{q_t}} + \beta(z_t^{\mathrm{d}_{q_t}} - z_t^{\mathrm{r}_{q_t}}))\right] - \tanh\left[\mu_{y_k} D_k y_t^{\mathrm{r}_k}\right])\right] - \tanh\left[\mu_{z_k} B z_t^{\mathrm{r}_k}\right]. \tag{22}$$

The differential coupling term, $\beta(z_t^{\mathrm{d}_{q_t}} - z_t^{\mathrm{r}_{q_t}})$ is now a random function of the states of all oscillators, but still serves to decouple the drive and response systems when the corresponding oscillator pairs are synchronized. The synchronization itself, however, does not depend on this differential term or where it came from. The only important point is this: the distribution of $z_t^{\mathrm{d}_{q_t}}$ must ensure that the transverse CLEs for $e_t^{y_k} = y_t^{\mathrm{d}_k} - y_t^{\mathrm{r}_k}$ are negative for all k. This will synchronize the y-maps, and, if α is chosen within the proper range, the z-maps will follow. The restriction on the coupling signal is very weak, since almost any distribution with broad support and a β value in the correct range will produce negative CLEs [42,43]. The fact that each oscillator pair is different is also of no consequence provided they all fall within a broad parameter range.

The scalar signal, $s_t = z_t^{\mathrm{d}_{q_t}}$, which is communicated from the drive to the response system is random by construction. If the number, N, of oscillator pairs is large enough, s_t tends towards white noise. Fig. 14 shows the return map

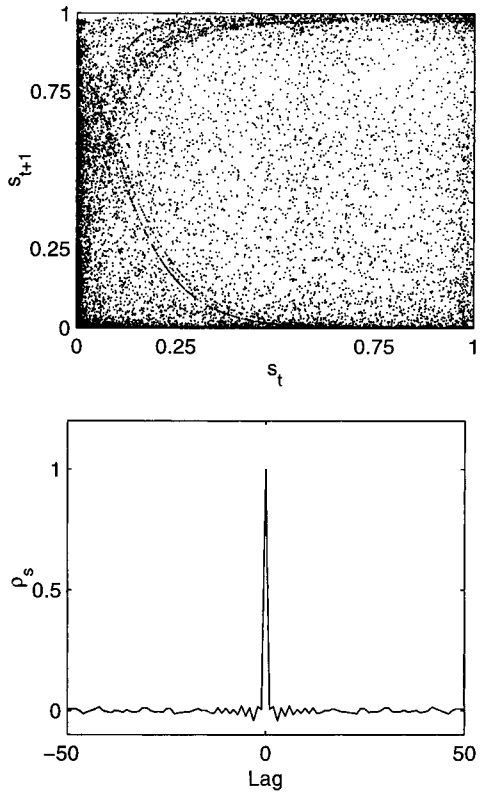

Fig. 14. Graph (a) (top) shows the 1-step return map for s_t in a 10-oscillator system. Graph (b) (bottom) shows the normalized autocorrelation function for the centered signal $s_t - \langle s_t \rangle$. The $(\mu_z/A/B, \mu_y/C/D)$ values for the oscillators were: 1 (5.0/5.0/1.0, 5.0/5.0/1.0); 2 (4.0/8.0/1.0, 6.0/6.0/1.0); 3 (7.0/5.0/1.0, 5.0/7.0/1.0); 4 (10.0/4.0/1.0, 5.0/5.0/1.0); 5 (5.0/9.0/1.0, 5.0/4.0/1.0); 6 (5.0/6.0/1.0, 7.0/5.0/1.0); 7 (5.0/4.0/1.0, 5.0/8.0/1.0); 8 (4.5/6.5/1.0, 6.5/4.5/1.0); 9 (7.5/6.5/1.0, 4.5/4.5/1.0); 10 (6.5/4.5/1.0, 4.5/6.5/1.0); note the space-filling structure of the signal, and the white noise-like autocorrelation.

and autocorrelation function for the coupling signal in a system of 10 oscillators. Very little structure is visible in this signal, and its autocorrelation is close to that of white noise. Nevertheless, as shown in Fig. 15, all 10 oscillators in the response population are synchronized with their driving counterparts. As pointed out in [36], such a coupling signal is potentially much better for secure communications than a simple chaotic signal which may be amenable to delay-coordinate and spectral reconstruction [57–59]. Possible communications applications for this system will be discussed elsewhere.

5. Synchronizing high-dimensional maps

All systems discussed above have been based on the two-dimensional map given by Eq. (10). However, the methods we describe are applicable to maps of any dimensionality constructed by chaining together several one-dimensional maps of type $z_{t+1} = f(z_t)$. In this section, we briefly illustrate such synchronization. Fig. 16 shows the drive and response systems, where corresponding maps have identical parameters. The drive system consists of M different maps with randomly chosen parameters. The dynamics of the system are given by

$$z_{t+1}^{\mathrm{d}_1} = f_1(z_t^{\mathrm{d}_1}, z_t^{\mathrm{d}_M}) = \tanh[\mu_1(A_1 z_t^{\mathrm{d}_1} + \alpha_1 z_t^{\mathrm{d}_M})] - \tanh[\mu_1 B_1 z_t^{\mathrm{d}_1}], \tag{23}$$

$$z_{t+1}^{\mathrm{d}_j} = f_j(z_t^{\mathrm{d}_j}, z_{t+1}^{\mathrm{d}_{j-1}}) = \tanh[\mu_j(A_j z_t^{\mathrm{d}_j} + \alpha_j z_{t+1}^{\mathrm{d}_{j-1}})] - \tanh[\mu_j B_j z_t^{\mathrm{d}_j}], \qquad j = 2, 3, 4, \ldots, M. \tag{24}$$

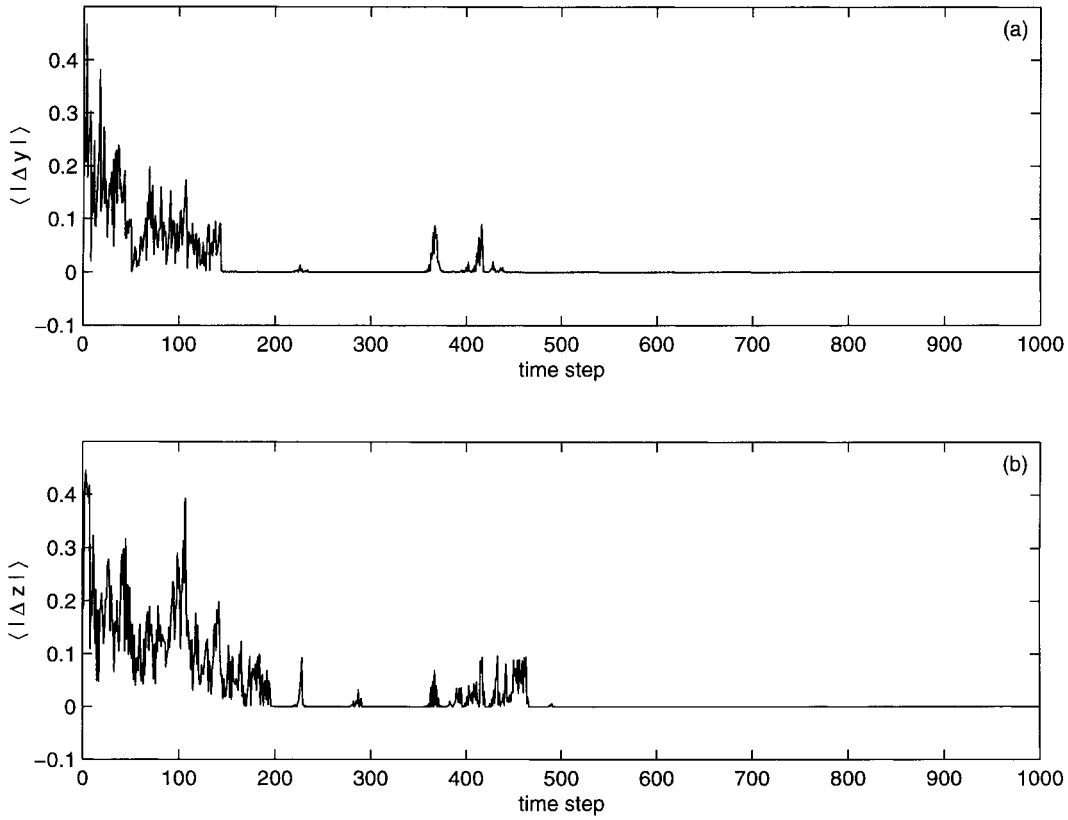

Fig. 15. Mean difference between the y-maps (Graph (a)) and z-maps (Graph (b)) of all oscillators in the system from Fig. 14. Full synchronization, achieved around step 500, remains stable thereafter.

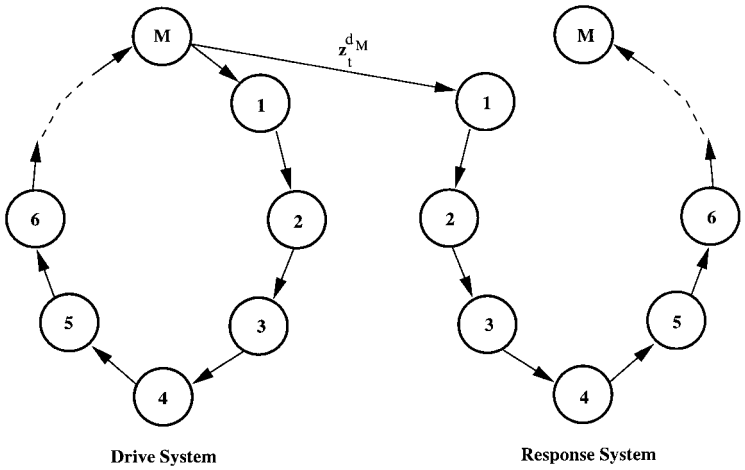

Fig. 16. Synchronizable system with high-dimensional maps. Each circle in the figure corresponds to a map of the type given by Eq. (5). Maps with identical numbers have identical parameters. The system corresponds to Eqs. (23)–(26).

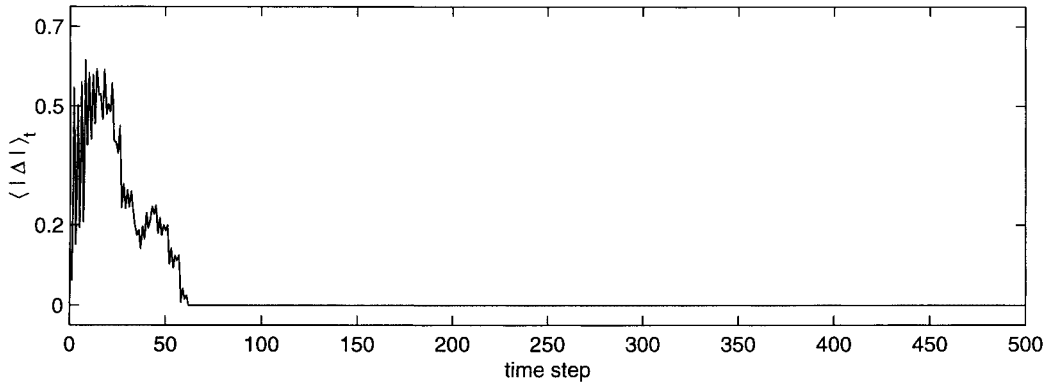

Fig. 17. Time series of mean error between corresponding elements in two 40-element systems. Parameters for the maps are selected randomly (see text).

Parameters for all maps are chosen randomly in the ranges $7.0 \leq \mu_j \leq 10.0$, $7.0 \leq A_j \leq 10.0$, $1.0 \leq B_j \leq 1.5$, and $0.25 \leq \alpha_j \leq 0.75$, so all maps in the system are different. The response system is identical in structure and parameter values, and has dynamics given by

$$z_{t+1}^{\mathrm{r}_1} = f_1(z_t^{\mathrm{r}_1}, z_t^{\mathrm{d}_M}) = \tanh[\mu_1(A_1 z_t^{\mathrm{r}_1} + \alpha_1 z_t^{\mathrm{d}_M})] - \tanh[\mu_1 B_1 z_t^{\mathrm{r}_1}], \tag{25}$$

$$z_{t+1}^{\mathrm{r}_j} = f_j(z_t^{\mathrm{r}_j}, z_{t+1}^{\mathrm{r}_{j-1}}) = \tanh[\mu_j(A_j z_t^{\mathrm{r}_j} + \alpha_j z_{t+1}^{\mathrm{r}_{j-1}})] - \tanh[\mu_j B_j z_t^{\mathrm{r}_j}], \qquad j = 2, 3, 4, \ldots, M. \tag{26}$$

Thus, the only coupling from the drive to response system is provided by $z_t^{\mathrm{d}_M}$. The system given by Eq. (10) corresponds to the $M = 2$ case. Fig. 17 shows the time series of the error, $\langle |\ \Delta\ | \rangle_t = M^{-1} \sum_j |\ z_t^{\mathrm{d}_j} - z_t^{\mathrm{r}_j}\ |$, for a $M = 40$ system. As in the $M = 2$ case, synchronization emerges rapidly through coalescence. The Jacobian for the error dynamics is lower triangular because of the serial structure of the drive and response systems, and the analysis for the $M = 2$ system applies directly for any M. Also, just as it was possible to synchronize arrays of $M = 2$ systems through a random scalar coupling, arrays of non-identical $M > 2$ systems can also be synchronized in the same way. The populations G^{d} and G^{r} in this case would consist of NM-dimensional maps. Many other synchronizable configurations are also possible, including series cascades, trees, and other non-recurrent arrangements of M-map systems.

6. Conclusion

In conclusion, we have demonstrated an extremely simple scheme for synchronizing unidirectionally coupled chaotic maps, and shown how it can be used to synchronize groups of different oscillators through a scalar coupling signal constructed randomly from the oscillator states. The coupling signal can carry a large number of multiplexed messages but has characteristics approximating white noise. Such a system could be very useful in applications such as secure communications. We have also described how our methods can be applied to high-dimensional maps.

Acknowledgements

The authors would like to thank Xin Wang, Tom Carroll, Kevin Short, Mingzhou Ding, Chai Wah Wu and Tao Yang for providing reprints of their work. This work was partially supported by a grant from The Ohio Board of Regents.

References

[1] L.M. Pecora, T.L. Carroll, Synchronization in chaotic systems, Phys. Rev. Lett. 64 (1990) 821–824.
[2] L.M. Pecora, T.L. Carroll, Driving systems with chaotic signals, Phys. Rev. A 44 (1991) 2374–2383.
[3] K.M. Cuomo, A.V. Oppenheim, Circuit implementation of synchronized chaos with applications to communications, Phys. Rev. Lett. 71 (1993) 65–68.
[4] K.M. Cuomo, A.V. Oppenheim, S.H. Strogatz, Synchronization of lorenz-based chaotic circuits with applications to communications, IEEE Trans. Circuits and Systems II 40 (1993) 626–633.
[5] C.W. Wu, L.O. Chua, A simple way to synchronize chaotic systems with applications to secure communication systems, Int. J. Bifure Chaos 3 (1993) 1619–1627.
[6] S. Hayes, C. Grebogi, E. Ott, Communicating with chaos, Phys. Rev. Lett. 70 (1993) 3031–3034.
[7] S. Hayes, C. Grebogi, E. Ott, A. Mark, Experimental control of chaos for communication, Phys. Rev. Lett. 73 (1994) 1781–1784.
[8] D.R. Frey, Chaotic signal encoding: An approach to secure communication, IEEE Trans. Circuits and Systems II 40 (1993) 660–666.
[9] H. Dedieu, M.P. Kennedy, M. Hasler, Chaos shift keying: Modulation and demodulation of a chaotic carrier using self-synchronizing chua's circuits, IEEE Trans. Circuits and Systems-II 40 (1993) 635–642.
[10] H.D.I. Abarbanel, P.S. Linsay, Secure communications and unstable periodic orbits of strange attractors, IEEE Trans. Circuits and Systems II 40 (1993) 643–645.
[11] T. Yang, Recovery of digital signals from chaotic switching, Int. J. Circuit Theory Appl. 23 (1995) 611–615 .
[12] L. Kocarev, U. Parlitz, General approach for chaotic synchronization with applications to communications, Phys. Rev. Lett. 74 (1995) 5028–5031.
[13] U. Parlitz, L. Kocarev, T. Stojanovski, H. Preckel, Encoding messages using chaotic synchronization, Phys. Rev. E 53 (1996) 4351–4361.
[14] T. Yang, L.O. Chua, Channel-independent chaotic secure communication, Int. J. Bifurc. Chaos 6 (1996) 2653–2660.
[15] T. Yang, L.O. Chua, Secure communication via chaotic parameter modulation, IEEE Trans. Circuits and Systems I 43 (1996) 817–819.
[16] J.H. Peng, E.J. Ding, M. Ding, W. Yang, Synchronizing hyperchaos with a scalar transmitted signal, Phys. Rev. Lett. 76 (1996) 904–907.
[17] Y.-C. Lai, C. Grebogi, Synchronization of spatiotemporal chaotic systems by feedback control, Phys. Rev. E 50 (1994) 1894–1899.
[18] L. Kocarev, U. Parlitz, T. Stojanovski, An application of synchronized chaotic dynamic arrays, Phys. Lett. A 217 (1996) 280–284.
[19] T. Yamada, H. Fujisaka, Stability theory of synchronized motion in coupled oscillator systems. ii – the mapping approach, Progr. Theoret. Phys. 70 (1983) 1240.
[20] A. Pikovsky, P. Grassberger, Symmetry breaking bifurcation for coupled chaotic attractors, J. Phys. A 24 (1991) 4587–4597.
[21] F.E. Udwadia, N. Raju, Some global properties of a pair of coupled maps: Quasi-symmetry, periodicity, and synchronicity, Physica D 111 (1998) 16–26.
[22] X. Wang, Discrete-time neural networks as dynamical systems, Ph.D. Thesis, University of Southern California, 1992.
[23] K. Kaneko, Spatiotemporal chaos in one-and two-dimensional coupled map lattices, Physica D 37 (1989) 60–82.
[24] K. Kaneko, Clustering, coding, switching, hierarchical ordering, and control in a network of chaotic elements, Physica D 41 (1990) 137–172.
[25] G. Keller, M. Künzle, T. Nowicki, Some phase transitions in coupled map lattices, Physica D 59 (1992) 39–51.
[26] V.I. Nekorkin, V.A. Makarov, V.B. Kazantsev, M.G. Veralde, Spatial disorder and pattern formation in lattices of coupled bistable elements, Physica D 100 (1997) 330–342.
[27] J.M. Kowalski, G.L. Albert, G.W. Gross, Asymptotically synchronous chaotic orbits in systems of excitable elements, Phys. Rev. A 42 (1990) 6260–6263.
[28] N. Nakagawa, Y. Kuramoto, Collective chaos in a population of globally coupled oscillators, Progr. Theoret. Phys. 89 (1993) 313–323.
[29] T. Kapitaniak, Transition to hyperchaos in chaotically forced coupled oscillators, Phys. Rev. E 47 (1993) R2975-R2978.
[30] L.M. Pecora, Synchronization conditions and desynchronizing patterns in coupled limit-cycle and chaotic systems, Phys. Rev. E. 58 (1998) 347–360.
[31] A. De Angeli, R. Genesio, A. Tesi, Dead-beat chaos synchronization in discrete-time systems, IEEE Trans. Circuits and Systems I 42 (1995) 44–56.
[32] L.S. Tsimring, M.M. Sushchik, Multiplexing chaotic signals using synchronization, Phys. Lett. A 213 (1996) 155–166.
[33] J. Güémez, M.A. Matías, Synchronous oscillatory activity in ensembles of chaotic model neurons, Physica D 96 (1996) 334–343.
[34] A.S. Dmitriev, M. Shirokov, S.O. Starkov, Chaotic synchronization in ensembles of coupled maps, IEEE Trans. Circuits Systems I 44 (1997) 919–926.
[35] M.M. Sushchik Jr., N.F. Rulkov, H.D.I. Abarbanel, Robustness and stability of synchronized chaos: An illustrative model, IEEE Trans. Circuits and Systems I 44 (1997) 867–873.
[36] L.M. Pecora, T.L. Carroll, G. Johnson, D. Mar, Volume-preserving and volume expanding synchronized chaotic systems, Phys. Rev. E 56 (1997) 5090–5100.
[37] T. Ushio, Chaotic synchronization and controlling chaos based on contraction mapping, Phys. Lett. A 198 (1997) 14–22.
[38] T.L. Carroll, L.M. Pecora, Synchronizing hyperchaotic volume preserving maps and circuits, IEEE Trans. Circuits and Systems I 45 (1998) 656–659.
[39] S.C. Venkataramani, B.R. Hunt, E. Ott, Bubbling transition, Phys. Rev. E 54 (1996) 1346–1360.
[40] T.L. Carroll, J.F. Heagy, L.M. Pecora, Transforming signals with chaotic synchronization, Phys. Rev. E 54 (1996) 4676–4680.

[41] L. Zonghua, C. Shigang, Synchronization of a conservative map, Phys. Rev. E 56 (1997) 1585–1589.
[42] A.A. Minai, T. Anand, Chaos-induced synchronization in discrete-time oscillators driven by a random input, Phys. Rev. E 57 (1998) 1559–1562.
[43] A.A. Minai, T. Anand, Using noise to synchronize chaotic neural oscillators, In: Proceedings of the International Joint Conference on Neural Networks, vol. 98, 1998, pp. 1466–1471.
[44] L. Yu, E. Ott, Q. Chen, Transition to chaos for random dynamical systems, Phys. Rev. Lett. 65 (1990) 2935–2948.
[45] L. Yu, E. Ott, Q. Chen, Fractal distribution of floaters on a fluid surface and the transition to chaos for random maps, Physica D 53 (1991) 102–124.
[46] A.S. Pikovsky, Statistics of trajectory separation in noisy dynamical systems, Phys. Lett. A 165 (1992) 33–36.
[47] X. Wang, Period-doublings to chaos in a simple neural network: An analytic proof, Complex Systems 5 (1991) 425–441.
[48] A.A. Minai, T. Anand, Stimulus-induced bifurcations in discrete-time neural oscillators, Biol. Cybernet. 79 (1998) 87–96.
[49] Y. Maistrenko, T. Kapitaniak, Different types of chaos synchronization in two coupled piecewise linear maps, Phys. Rev. E 54 (1996) 3285–3292.
[50] Y. Maistrenko, V.L. Maistrenko, A. Popovich, E. Mosekilde, Transverse instability and riddled basins in a system of two coupled logistic maps, Phys. Rev. E 57 (1998) 2713–2724.
[51] E. Ott, J.C. Sommerer, Blowout bifurcations: The occurrence of riddled basins and on-off intermittency, Phys. Lett. A 188 (1994) 39–47.
[52] L. Longa, E.M.F. Curado, F.A. Oliviera, Roundoff-induced coalescence of chaotic trajectories, Phys. Rev. E 54 (1996) R2201–R2204.
[53] G. Malescio, Noise and synchronization in chaotic systems, Phys. Rev. E 53 (1996) 6551–6554.
[54] A. Maritan, J.R. Banavar, Chaos, noise and synchronization, Phys. Rev. Lett. 72 (1994) 1451–1454.
[55] A.A. Minai, T.D. Pandian, Communicating with noise: How chaos and noise combine to generate secure encryption keys, CHAOS, 1998, to appear.
[56] J.H. Xiao, G. Hu, Z. Qu, Synchronization of spatiotemporal chaos and its application to multichannel spread-spectrum communications, Phys. Rev. Lett. 77 (1996) 4162–4165.
[57] K.M. Short, Steps toward unmasking secure communications, Int. J. Bifurc. Chaos 4 (1994) 959–977.
[58] G. Peréz, H.A. Cerdeira, Extracting messages masked by chaos, Phys. Rev. Lett. 74 (1995) 1970–1973.
[59] K.M. Short, Unmasking a modulated chaotic communications scheme, Int. J. Bifurc. Chaos 6 (1996) 367–375.